JOURNAL OF MATERIALS SCIENCE 30 (1995) 3449–3456

The influence of cathodic hydrogen charging on the mechanical behaviour of Al–4Zn–1Mg alloy

C. PANAGOPOULOS, P. PAPAPANAYIOTOU
Laboratory of Physical Metallurgy, National Technical University of Athens, Zografou Campus, 15780, Athens, Greece

The effect of cathodic charging on the mechanical behaviour of Al–4Zn–1Mg alloy was studied. Hardening of the Al–4Zn–1Mg alloy surface, due to the hydrogen absorption, was observed. The ultimate tensile stress of the charged aluminium alloy was noted to be a non-linear function of the charging current density. The cathodically charged aluminium alloy exhibited brittle transgranular fracture at the surface layer, whereas ductile intergranular fracture was observed at the deeper layers of the same alloy.

1. Introduction

Hydrogen may be introduced into metallic materials during casting, acid pickling, electroplating, welding and corrosion processes. Hydrogen is mainly present in metallic materials in the form of interstitial atoms. These atoms can occupy either tetrahedral or octahedral positions ($r_t = 0.036$ nm and $r_o = 0.059$ nm, respectively) [1] of the lattice due to their small size ($r = 0.025$–0.054 nm) and can move rapidly either by diffusion or by transportation through mobile line defects. The influence of hydrogen is closely related to the metallic material's strength, its microstructure, the applied stress, the percentage of prior cold work and the degree of segregation of impurities at the grain boundaries [2].

The most recent publications dealing with the cathodic charging and the mechanical behaviour of some metallic materials are given below.

Bond *et al.* [3] studied the effect of cathodic hydrogen charging on the deformation behaviour of pure aluminium and noticed that hydrogen increases the dislocation mobility and reduces the flow stress of aluminium.

The cathodic hydrogen charging of pure aluminium was found, by Watson and co-workers [4], to decrease the ductility and increase the yield and ultimate tensile strength of this material, while the formation of a hardened surface layer was also observed.

Christodoulou and Flowers observed that in Al–Zn–Mg alloys, in the presence of hydrogen, intergranular fracture occurs, resulting in reduced fracture strain [5].

Lastly, Lynch studied the transcrystalline fracture of a high strength Al–6%Zn–3%Mg in a number of environments. The metallographic and fractographic studies of the transcrystalline fracture led Lynch to the conclusion that environmentally assisted cracking involves adsorption of hydrogen which facilitates the nucleation of dislocations at crack tips [6].

Although many models describing certain metal–hydrogen systems have been presented, a generally accepted model describing and predicting the metal–hydrogen interaction has not been developed yet. The purpose of this study is to investigate the effect of cathodic hydrogen charging on some mechanical properties of an Al–4%Zn–1%Mg alloy.

2. Experimental procedure

The material used was an Al–4%Zn–1%Mg alloy supplied in the form of cold-rolled sheet of 2.5 mm thickness. The samples were homogenized at 450 °C for 2 h, quenched in water at 10 °C and then aged at 100 °C for 24 h. This thermal treatment was performed for each specimen before the experiment in order to avoid different primary properties for each specimen due to natural ageing. The specimens were immediately subjected to chemical etching in a solution of 95% H_2O, 2.5% HNO_3, 1.5% HCl and 1% HF, then rinsed with acetone and blown dry under hot air current, prior to cathodic charging.

Cathodic charging was carried out in a solution of 75% CH_3OH, 22.4% H_2O, 2.6% H_2SO_4 and contained 10 mg l^{-1} As_2O_3 as hydrogen recombination inhibitor. The specimens were charged on both the front and back surfaces, with the use of graphite anodes. The charging current densities employed were in the range 10–90 mA cm^{-2} for the tensile tests and 40–95 mA cm^{-2} for the microhardness tests, while the charging time was varied from 3 to 35 h and from 6 to 30 h, respectively.

Mechanical testing was carried out immediately after charging to minimize the loss of hydrogen. The gauge sections for the tensile tests were $50 \times 10 \times 2.5$ mm. The tension tests were performed at a strain rate of 3.3×10^{-4} s^{-1}. One series of testing, however, involved the variation of strain rate from 3.3×10^{-4} s^{-1} to 1.7×10^{-2} s^{-1}. Microhardness testing was made with Vickers indenter imposing a 0.20 N load for 30 s. Each measurement was the average of eight indentations. Roughness tests were also carried out throughout the surface of the cathodically charged

0022–2461

specimens as well as that of the fractured ones, with the use of a Perthen profilometer. Each measurement was the average of five pre-measurements.

The surface of both the cathodically charged and the fractured specimens were examined with a Jenavert optical microscope. The fractured area of the subjected to tension specimens were examined with the use of a Philips scanning electron microscope (SEM).

3. Results and discussion

3.1. Optical microscopy

The surface of the charged specimens is covered with a dark grey coloured film (Fig. 1) the thickness of which increases as a function of both the charging time and the charging current density. This film is believed to be As, which was deposited during charging of the specimen [7,8]. A small degree of pitting, due to acid pickling of the specimens prior to their charging, can also be observed.

3.2. Microhardness tests

Microhardness tests on the surface of the specimens revealed major surface hardening due to charging. Microhardness continuously increases as a function of charging current density (I_{CD}) and charging time (t_{CH}). The maximum percentage increase of microhardness (Figs 2 and 3) always referring to that of the uncharged specimen (charging current density $I_{CD} = 0$ or charging time $t_{CH} = 0$, respectively), is $\Delta(MH)_{I_{CD}} = 67.9\%$, for $MH = f(I_{CD})$ and t_{CH} = constant and $\Delta(MH)_{t_{CH}} = 70.9\%$, for $MH = f(t_{CH})$ and I_{CD} = constant.

This significant influence of hydrogen on microhardness can be explained in terms of the dislocation pinning mechanism. Surface hardening must be attributed to solute hydrogen and dislocation pinning at the surface region. Solute hydrogen atoms act as dislocation pinning sites contributing to the work hardening of the alloy.

Conclusively, the increase of microhardness is due to decreased dislocation mobility. Higher charging current density leads to higher hydrogen fugacity while higher charging time leads to higher solute hydrogen concentration, both leading to more effective pinning of the dislocations and, therefore, decreased dislocation mobility.

Microhardness of the Al–4Zn–1Mg alloy is related to the time passed from the time of charging (Fig. 4). The reason for the decrease of the microhardness value during natural ageing is the gradual diffusion of hydrogen out of the specimen to the environment. The time necessary for this process to be completed is much greater than the time needed for hydrogen penetration. The reason is that hydrogen atoms are trapped in the metallic structure and that detrapping is the rate-controlling step of the hydrogen diffusion process. The hydrogen atoms still remaining in the specimen are probably irreversibly trapped and determine the microhardness value of the specimen. Their removal may be achieved either with long-term natural ageing or, even better, with appropriate thermal treatment in vacuum.

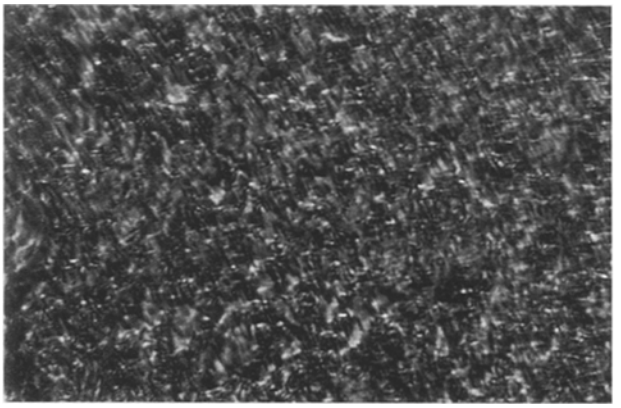

Figure 1 The surface of a specimen, cathodically charged at 40 mA cm^{-2} for 18 h, is covered with a dark As film.

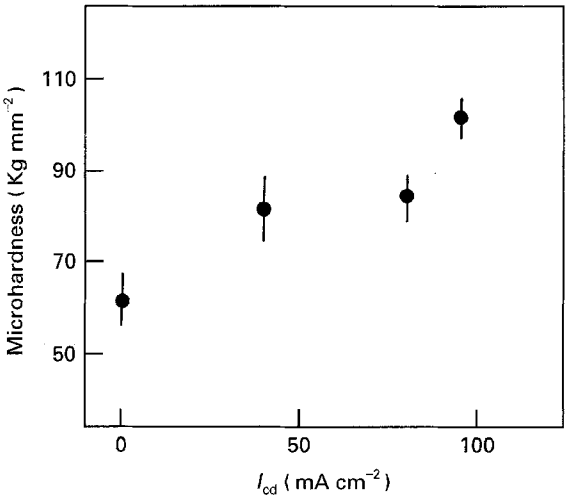

Figure 2 Effect of charging current density on the microhardness of Al–4Zn–1Mg alloy charged with hydrogen for 6 h.

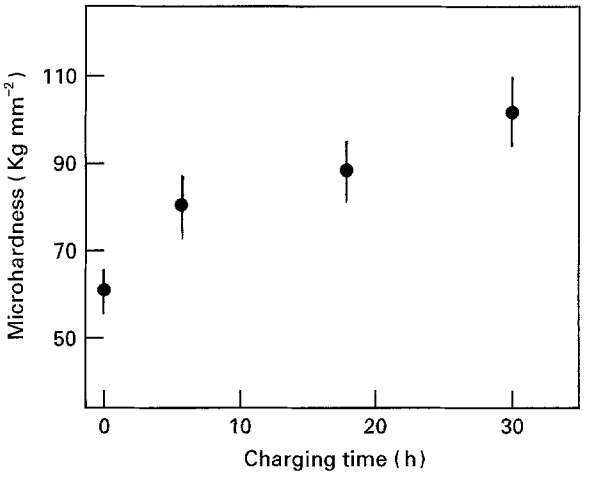

Figure 3 Effect of charging time on the microhardness of Al–4Zn–1Mg alloy charged with hydrogen at 40 mA cm^{-2}.

3.3. Tension tests

The influence of cathodic hydrogen charging on the tensile properties of the Al–4Zn–1Mg alloy is

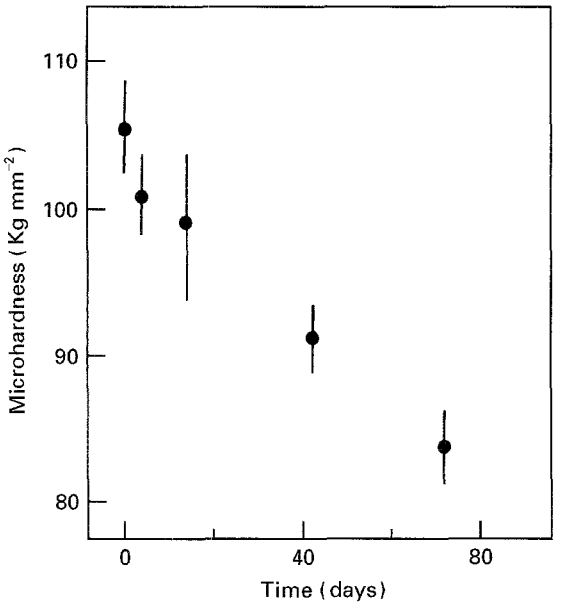

Figure 4 Effect of time passed beyond charging on the surface microhardness of a specimen charged at 40 mA cm^{-2} for 30 h.

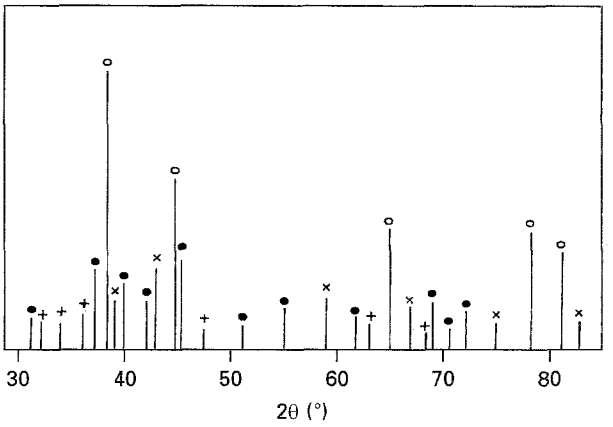

Figure 5 X-Ray diffraction diagram for Al–4Zn–1Mg alloy, charged at 80 mA cm^{-2} for 10 h. AlH_3 and free Mg were detected: o Al; + Mg; • $MgZn_2$; × AlH_2.

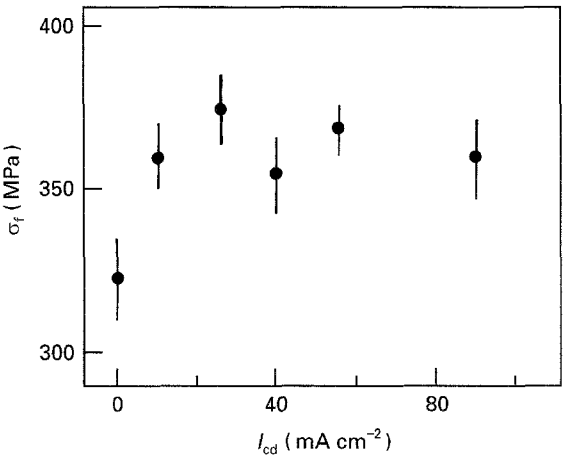

Figure 6 Effect of charging current density on the ultimate tensile stress of Al–4Zn–1Mg alloy charged for 3 h. Strain rate 3.3×10^{-4}.

complex. When hydrogen is introduced into the specimen it concentrates both at grain boundaries and in the interior of the grains. Hydrogen concentration in the interior of the grains, though, is much lower than that at the grain boundaries as a result of the low diffusivity and solubility of hydrogen in the metal matrix. The following equation [10] relates the apparent diffusivity of hydrogen (D) in a metal of trap density (N_t) and the diffusivity of hydrogen in a metal "free of traps" (D_o)

$$D_o/D = 1 + (k/p)\,N_t \qquad (1)$$

where k and p are trapping and detrapping parameters, respectively. According to this equation when trap density increases the apparent diffusivity of hydrogen is lowered, due to trapping effects [7]. These traps may be microvoids, precipitates, dislocations and grain boundaries. When the specimen is being deformed, hydrogen atoms are conveyed, mainly by mobile dislocations [11], towards these traps where they form molecular hydrogen in the form of bubbles. In our case (cathodic charging of the Al–4Zn–1Mg alloy) hydrogen atoms can not be trapped by the possibly existing $\eta'(MgZn_2)$ precipitate particles [12]. On the contrary, they are trapped along the incoherent matrix-η phase interface. The X-ray diffraction diagram (Fig. 5) of a charged specimen showed that free Mg is present, which is believed to be trapped along the grain boundaries while no free Zn was observed. This means that all Zn is present in the $MgZn_2$ phase. Previous research results on Al–Zn–Mg alloys [11, 13] are in accordance with this observation. Free Mg is believed to trap hydrogen atoms with electronic forces causing local supersaturation to occur. MgH and MgH_2 complex formations have also been cited. This trapping seems to be enhanced by previous heat treatment in the temperature range of 100–150 °C. Lastly, high angle grain boundaries are considered strong traps but this is not the case in Al–Zn–Mg alloys [12, 14].

In the first series of experiments the influence of the charging current density on the tensile behaviour of the charged specimens is studied (Fig. 6). The fracture mode for the uncharged specimen is completely transgranular ductile (Fig. 7) and results from internal void nucleation, growth and linking up, either by void impingement or by void sheets among grown voids (Fig. 8). The plastic flow is macroscopically uniform. For values of the current density up to 25 mA cm^{-2} the ultimate tensile strength increases. The role of hydrogen consists in the hardening of the alloy both by reducing dislocation mobility and by causing work-hardening of the material due to increased dislocation density, according to the mechanism already described. It is observed, however, that the fracture mode of the surface layer is brittle transgranular (Figs 9 and 10). This change of fracture mode can be attributed to the exceeding of a critical value of hydrogen concentration in the grain interior, $C_{(GI)cr}$, for this surface layer, beyond which dislocations are most effectively pinned by hydrogen atoms. On the fractured surface small voids are visible, which must have come from the formation of molecular hydrogen. The transgranular front (Fig. 10) indicates the point beyond which hydrogen concentration in the grain interior is lower than $C_{(GI)cr}$. This critical value has not

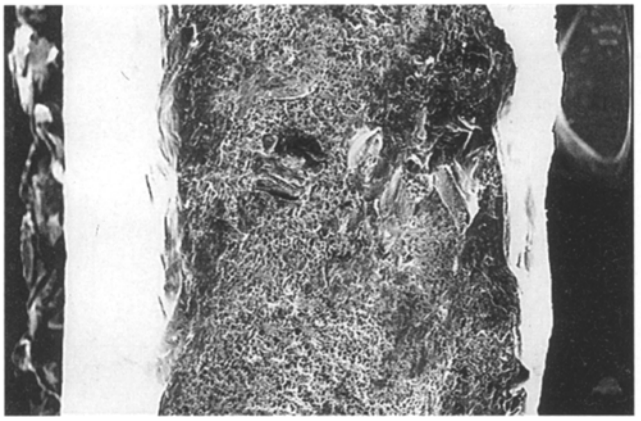

Figure 7 Micrograph of the fractured area of an uncharged specimen. Ductile transgranular fracture (× 42.6).

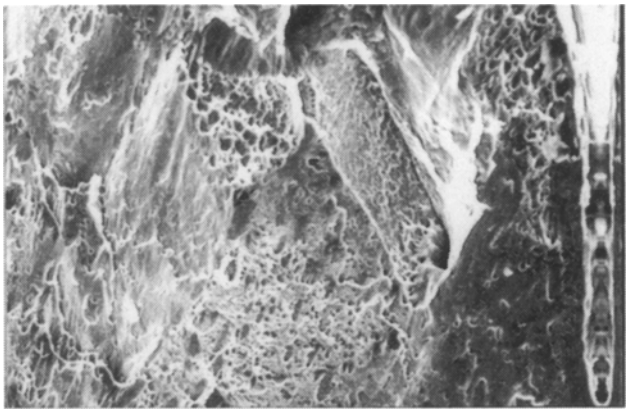

Figure 8 Micrograph of the fractured area of an uncharged specimen. Dimples and void sheets are observed (× 170).

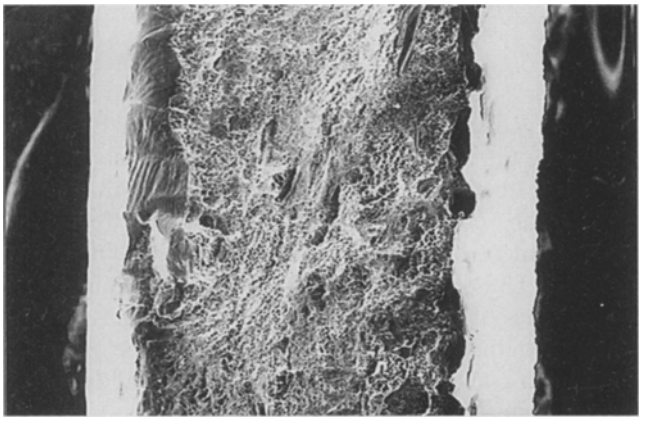

Figure 9 Micrograph of a specimen charged at 25 mA cm^{-2} for 3 h. Brittle transgranular fracture occurs near the surface (× 42.6).

been reached for deeper regions of the specimen because the hydrogen concentration profile is very steep, as already discussed.

When the charging current density further increases consecutively to 40, 55 and 90 mA cm^{-2} the ultimate tensile strength is approximately constant. Higher current density leads to higher hydrogen fugacity, resulting in higher hydrogen concentration for a given distance from surface. Hydrogen primarily concentrates along grain boundaries and matrix–precipitates interfaces, rather than the grain's interior. The resistance of the Al–4Zn–1Mg alloy to plastic flow is expected to decrease owing to hydrogen [15]. Local hydrogen pressure continuously increases since local hydrogen concentration increases, thus creating a stress field in the matrix. When a critical value of grain boundary hydrogen concentration $C_{(GB)cr}$ is reached, plastic deformation is localized at slip bands. Hydrogen is then conveyed by mobile dislocations to these regions, where slip bands terminate, which act as strongly irreversible traps. This leads to the conclusion that regions where greater slip is observed will have higher hydrogen concentration and suffer greater damage. Slip selectively occurs along the precipitate free zones. When the hydrogen pressure increases microcracks are formed along the precipitate free zones, acting as crack-initiation sites. Damage is greater when the precipitated phase is less coherent [16] and since the η phase is incoherent, damage is expected to be significant. The initial supply of lenticular voids may also come from dislocation pile-ups along the grain boundaries, which often aid the matrix–precipitate decohesion [17]. The voids so formed serve as precipitation sites of solute hydrogen.

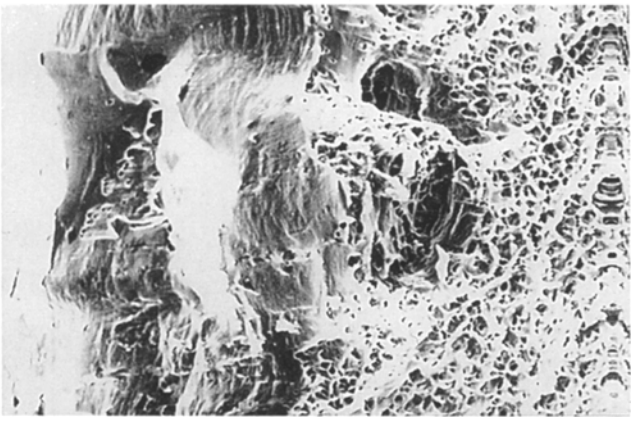

Figure 10 Micrograph of a specimen charged at 25 mA cm^{-2} for 3 h. The boundary between brittle and ductile fracture is observed (× 170).

Nucleation of voids ahead of cracks generally occurs in regions where plastic deformation is markedly inhomogeneous and separation of particle–matrix interfaces or fracture of brittle particles is usually involved. It is clear that the first two presuppositions are valid. As regards the fracture of brittle particles, the formation of Al and Mg hydrides has been proposed [15]. This assertion was not verified for Mg by X-ray diffraction examination. Besides, these combinations are unstable in humid environments such as the laboratory room. However, AlH_3 was detected by the X-ray examination (Fig. 5) which means that part of the crack-growth mechanism could be the fracture of platelike AlH_3 formations along the grain boundaries, which is still of little importance. The crack growth mechanism primarily consists in the coalescence of voids with the external crack. This process is aided by the nucleation of dislocations, which is partly due to the presence of trapped hydrogen and their subsequent movement from both the crack tip and the

voids [16]. It is assumed that nucleation of dislocations is a more difficult process than their subsequent movement and that the local shear stress is sufficient for their continued movement once nucleation has occurred. Any localization of this kind results in a local increase in strain rate. Fracture is therefore accompanied by large local slip.

Cracks along the grain boundaries at the region of intergranular fracture of a specimen charged at 55 mA cm^{-2} are observed in Fig. 11. Ductile transgranular fracture has also occurred.

Nucleation and growth of voids around the precipitated particles due to stress localization results in the development of dimpled intergranular fractured surfaces of the Al–4Zn–1Mg alloy. When precipitate free zones are very narrow, strains are so highly localized that dimples are extremely shallow and thus difficult to detect [18]. This is the case here since high resolution was used (×5200) (Fig. 12) in order to detect dimples on the apparently flat grain-boundary facets. In Fig. 13 spherical voids along the grain boundaries are observed. High hydrogen pressure imposed a stress field on the surrounding matrix, and this is verified by the fact that matrix is locally deformed for a distance around the voids equal to ten times their radius.

According to the fracture mechanism described above it is clear that a further increase of the charging current density will lead to the progress of the intergranular front deeper into the specimen (Figs 14 and 15) which means that the percentage of intergranular fracture mode, throughout the whole fractured surface, increases. The critical stress for intergranular fracture is lower than the critical stress for transgranular fracture, thus imposing a limit to the ultimate tensile stress. Therefore, the ultimate tensile stress of the specimen takes its maximum value and becomes approximately constant when a critical current density value is reached, for which the positive influence of hydrogen on the ultimate tensile stress (higher fracture stress for regions of ductile transgranular fracture mode) is balanced by the negative influence of hydrogen on the ultimate tensile stress (increasing percentage of IG fracture mode). This critical value appears to be more than 25 mA cm^{-2} and less than 40 mA cm^{-2}. An important observation is the existence of a transgranular crack at the point of convergence of three grains (Fig. 16). This may be attributed to the damaging effect of hydrogen at regions of high triaxility.

The change of the maximum elongation as a function of the charging current density (Fig. 1) is adverse

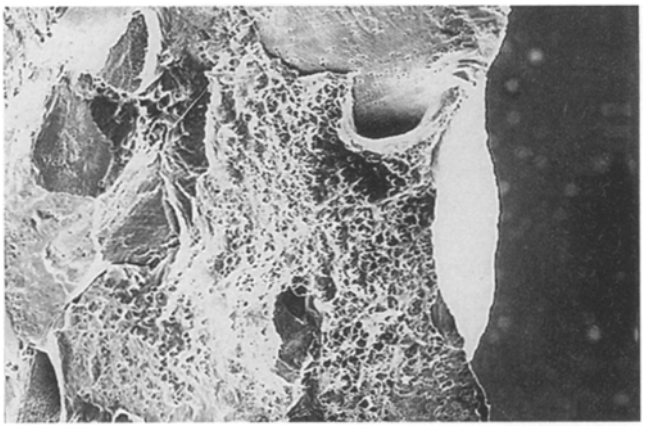

Figure 11 Micrograph of a specimen charged at 55 mA cm^{-2} for 3 h. IG fractured areas among transgranular fractured areas. Cracks along the grain boundaries can be observed (×85).

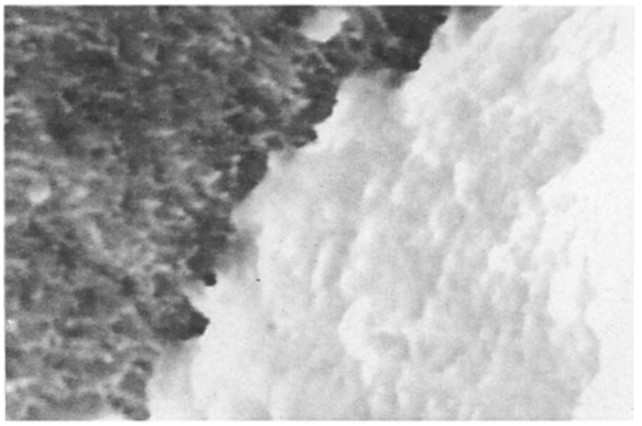

Figure 12 Micrograph of a specimen charged at 90 mA cm^{-2} for 3 h. Grain boundary facets (intergranularly fractured area) covered with very shallow dimples (×5200).

Figure 13 Micrograph of a specimen charged at 90 mA cm^{-2} for 3 h. Spherical voids along the grain boundaries, formed as a result of high local concentration of hydrogen. A high stress field is developed around each of them (×655).

Figure 14 Micrograph of a specimen charged at 55 mA cm^{-2} for 3 h. Areas of ductile intergranular and ductile intergranular fracture (×42.6).

Figure 15 Micrograph of a specimen charged at 90 mA cm^{-2} for 3 h. Intergranular fracture has propagated. Brittle transgranular fracture is limited near the surface (×42.6).

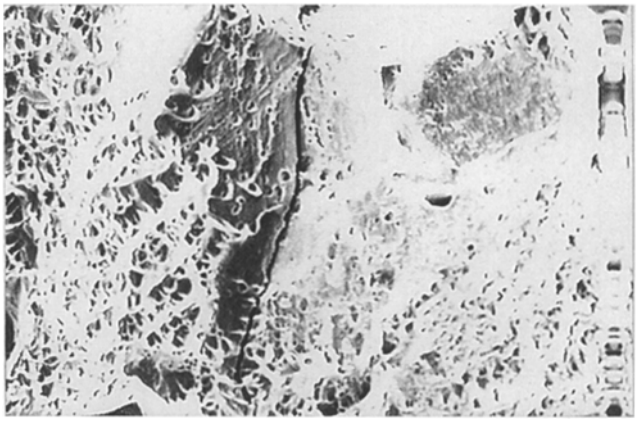

Figure 16 Micrograph of a specimen charged at 90 mA cm^{-2} for 3 h. Transgranular crack owing to the damaging effect at regions of high triaxility (×170).

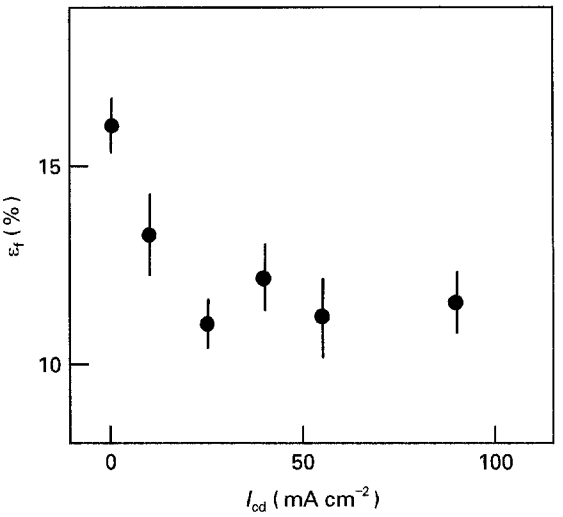

Figure 17 Effect of charging current density on the maximum tensile elongation of Al–4Zn–1Mg alloy charged at 25 mA cm^{-2} for 3 h. Strain rate 3.3×10^{-4} s^{-1}.

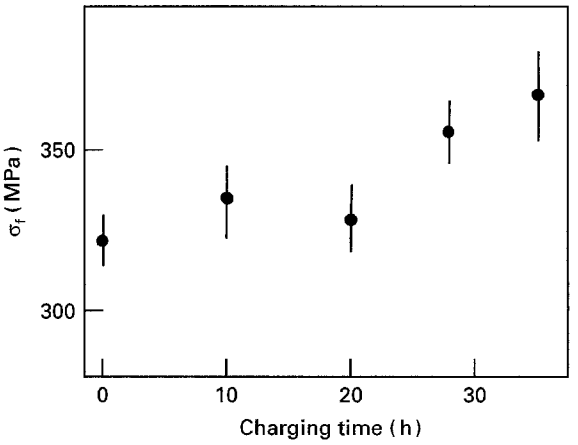

Figure 18 Effect of charging time on the ultimate tensile stress of Al–4Zn–1Mg alloy charged with hydrogen at 25 mA cm^{-2}. Strain rate 3.3×10^{-4} s^{-1}.

to the change of the ultimate tensile strength. Maximum elongation initially decreases owing to the hardening of the alloy and then slightly increases. This increase may be ascribed to the extensive local slip observed along the grain boundaries.

The influence of the charging time on the tensile behaviour of Al–4Zn–1Mg alloy can be explained in terms of the fracture mechanism described above. It must be pointed out that charging time does not affect hydrogen concentration of the saturated surface layer and hydrogen fugacity. The results obtained for the specimen charged for 3 h have already been discussed. Since hydrogen diffusivity in the matrix is very low and hydrogen diffusion is the rate-controlling step, when charging time is further increased hydrogen atoms diffuse deeper into the specimen. The critical hydrogen concentration $C_{(GI)cr}$ for the grain interior is then reached for a greater distance from the surface of the specimen, causing the brittle transgranular fracture zone to expand inwards. Since for the 25 mA cm^{-2} transgranular (ductile and brittle) fracture only occurs (Fig. 9) it may be assumed that hydrogen fugacity is not high enough for ductile intergranular fracture to occur. The increase of the ultimate tensile stress (Fig. 18) is then primarily due to the advance of the brittle transgranular fracture front (and the consequent increase of the brittle transgranular fracture mode percentage throughout the fractured area), and the hardening of the alloy in the regions that exhibit ductile fracture. Maximum elongation appears to be practically stable (Fig. 19) which is unexpected. A study of the fracture elongation might have shown that fracture elongation decreases as a function of charging time, as was initially expected.

Lastly, the influence of the strain rate on the ultimate tensile stress of the Al–4Zn–1Mg alloy was studied (Fig. 20). The ultimate tensile strength initially decreases for values of strain rate greater than approximately 10^{-3} s^{-1} and then becomes stable. When strain rate is low, mobile dislocations can capture hydrogen atoms and carry them away. The cores of dislocation are heavily distorted regions in the crystal lattice, which causes a strong strain field. When hydrogen atoms fill this region, they will relax the strain field and result in a decrease of distortion energy; therefore, dislocation cores are strong hydrogen traps, so that hydrogen atoms along dislocation lines will be trapped by dislocation cores and then carried away to grain boundaries and interfaces of precipitates.

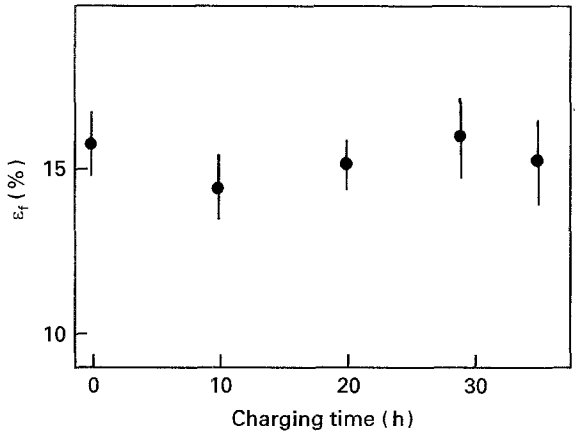

Figure 19 Effect of charging time on the maximum tensile elongation of Al–4Zn–1Mg alloy charged with hydrogen at 25 mA cm^{-2}. Strain rate 3.3×10^{-4} s^{-1}.

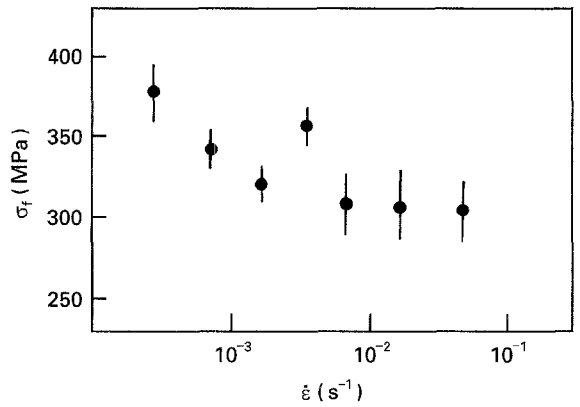

Figure 20 Effect of strain rate on the ultimate tensile stress of Al–4Zn–1Mg alloy charged with hydrogen at 25 mA cm^{-2} for 3 h.

The critical velocity V_c for breakaway of core atmosphere is

$$V_c = 3.2(D_H/\alpha) \quad (2)$$

where D_H is the diffusivity of hydrogen atom in matrix (taken approximately as 10^{-14} m^2 s^{-1}) and α is the radius of a dislocation core, taken as $\boldsymbol{b}$, Burger's vector. The critical strain rate ε_c of specimens is given as

$$\varepsilon_c = \rho_H \boldsymbol{b} V_c \quad (3)$$

where ρ_H is the mobile dislocation density, taken as 10^6 cm^{-2}. By combining Equations 2 and 3

$$\varepsilon_c = 3.2(\rho_H D_H) = 3.2 \times 10^{-4}\ s^{-1} \quad (4)$$

When strain rate exceeds this critical value, the hydrogen atoms trapped by the dislocation core break away from it. The energy of each mobile dislocation is so high that pinning of mobile dislocations by hydrogen atoms does not occur. Thus, since the alloy is not hardened, hydrogen influence on the ultimate tensile strength is rather insignificant for strain rates higher than the critical value. It appears in this case that $\dot{\varepsilon}_c$ is higher (approximately 10^{-3} s^{-1}) than it was theoretically estimated to be.

4. Roughness tests

Roughness tests were carried out on the surface of the charged specimens of the Al–4Zn–1Mg alloy. Roughness R_a, generally increases when charging current density I_{CD} increases (Fig. 21). For the fractured specimens roughness is greater at the neck region (distance from the point of fracture 1 cm) compared to that counted 2 cm or more, far from the point of fracture (Fig. 22). The reason is that from the moment the neck has formed, deformation of the specimen occurs almost exclusively at this region, and the surface of the specimen becomes very rough. Roughness is greatly related to the relative slide of adjoining grains and it is also related to the formation of microcracks on the surface of the fractured specimens. For charging current density values less than 25 mA cm^{-2} the effect of hydrogen is only to harden the metal matrix and the surface layer exhibits ductile transgranular fracture,

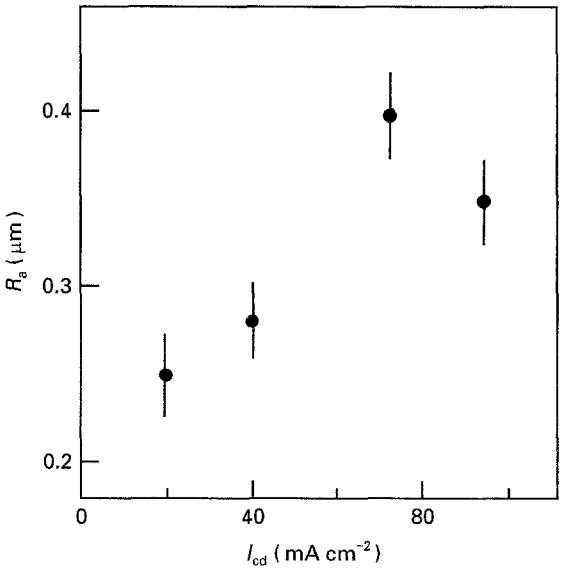

Figure 21 Effect of charging current density on the roughness of the specimens charged for 6 h.

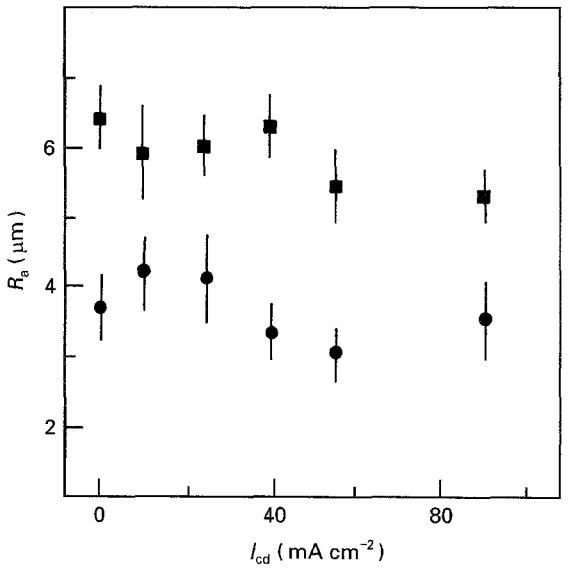

Figure 22 Effect of charging current density on the roughness of the fractured specimens charged for 6 h. Strain rate 3.3×10^{-4} s^{-1}.

just as the whole specimen does. When current density exceeds 25–40 mA cm^{-2} (which leads to brittle transgranular fracture of the surface layer) surface grains are less able to slide, and roughness decreases. Microcracks are formed because of the embrittlement of the matrix, which can not deform plastically, as it does when the hydrogen concentration is lower. So when the maximum stress applied is higher, microcrack density is higher as a result. Another reason for the formation of microcracks may be that the inner part of the specimen tends to deform more than the embrittled surface layer does. This difference in deformability causes additional tensile stresses to develop upon the embrittled surface layer, aiding the formation of microcracks.

5. Conclusions

1. Cathodic hydrogen charging affects the tensile behaviour of the Al–4Zn–1Mg alloy. There is a critical hydrogen concentration in the grain interior $C_{(GI)cr}$, which signals the transition from ductile transgranular to brittle transgranular fracture mode. This critical concentration is reached only for a layer near the surface of the specimen.
2. When a critical hydrogen concentration along the grain boundaries $C_{(GB)cr}$ is reached, the fracture mode changes from ductile transgranular to ductile intergranular.
3. Ductile transgranular fracture was accompanied by extensive local slip along the grain boundaries. Grain boundary facets are covered with very shallow dimples and slip bands can be observed.
4. The ultimate tensile stress of the Al–4Zn–1Mg becomes maximum (as a function of charging current density) when the positive influence of hydrogen on the strength of the alloy (hardening of the regions that exhibit ductile transgranular fracture) is balanced by the negative one (increase of the percentage of intergranular fractured area). The current density value for which this occurs is approximately 25 mA cm^{-2}.
5. Longer charging time leads to advance of the brittle transgranular front inwards, resulting in an increase of the ultimate tensile strength.
6. There is a critical strain rate ε_c beyond which the breakaway of the hydrogen atmosphere of the dislocation core occurs, and mobile dislocations are not pinned by solute hydrogen atoms. This leads to a decrease of the ultimate tensile strength.
7. The surface of the Al–4Zn–1Mg was hardened considerably. The surface layer did not recover to its prior-to-charging hardness with the time passed after charging.
8. As shown by the X-ray diffraction results, AlH_3 formation was detected. This hydride may participate in the fracture mechanism.

References

1. I. O. SHIM and J. G. BYRNE, *Mater. Sci. Eng.* **74** (1985) 174.
2. V. KERLINS, "Metals Handbook, Vol. 12, Fractography", 9th edition (ASM, Metals Park, OH, 1987) p.13.
3. G. M. BOND, I. M. ROBERTSON and H. K. BIRNBAUM, *Acta Metall.* **36** (1988) 2193.
4. J. W. WATSON, Y. Z. SHEN and M. MESHII, *Met. Trans.* **19A** (1988) 2299.
5. L. CHRISTODOULOU and H. M. FLOWER, *Acta. Metall.* **28** (1980) 481.
6. S. P. LYNCH, *Corrosion Sci.* **22** (1982) 925.
7. S. NAKAHARA and Y. OKINAKA, *J. Electrochem. Soc.* **136** (1989) 1892.
8. A. KIMURA and H. K BIRNBAUM, *Acta Metall.* **35** (1987) 1077.
9. L. CHEN, W. CHEN, Z. LIU, Y. SHAO and Z. HU, *Met. Trans.* **24A** (1993) 1355.
10. R. M. LATANISION and M. KURKELA, *Corrosion* **39** (1983) 174.
11. J. ALBRECHT, A. W. THOMPSON and I. M. BERNSTEIN, *Met. Trans.* **10A** (1979) 1759.
12. Y. IIJIMA, S. I. YOSHIDA, H. SAITOH, H. TANAKA and K. I. HIRANO, *J. Mater. Sci.* **27** (1992) 5735.
13. R. K. VISWANADHAM, T. S. SUN and J. A. S. GREEN, *Met. Trans.* **11A** (1980) 85.
14. J. YAO, S. A. MEGUID and J. R. CAHOON, ibid. **24 A** (1993) 105.
15. F. ZEIDES and I. ROMAN, *Mater. Sci. Eng.* **A125** (1990) 21.
16. D. KWON, S. LEE and R. J. ASARO, *Met. Trans.* **23A** (1991) 1375.
17. H. P. VAN LEEUWEN, *Corrosion* **29** (1973) 197.
18. S. P. LYNCH, *Acta Metall.* **29** (1981) 325.

Received 23 February 1994
and accepted 20 January 1995